

Imitation Learning from Purified Demonstrations

Yunke Wang¹, Minjing Dong², Bo Du¹, Chang Xu²

¹School of Computer Science, Institute of Artificial Intelligence, Wuhan University

²School of Computer Science, Faculty of Engineering, The University of Sydney

{yunke.wang, dubo}@whu.edu.cn, mdong0736@uni.sydney.edu.au, c.xu@sydney.edu.au

Abstract

Imitation learning has emerged as a promising approach for addressing sequential decision-making problems, with the assumption that expert demonstrations are optimal. However, in real-world scenarios, expert demonstrations are often imperfect, leading to challenges in effectively applying imitation learning. While existing research has focused on optimizing with imperfect demonstrations, the training typically requires a certain proportion of optimal demonstrations to guarantee performance. To tackle these problems, we propose to purify the potential perturbations in imperfect demonstrations and subsequently conduct imitation learning from purified demonstrations. Motivated by the success of diffusion models, we introduce a two-step purification via the diffusion process. In the first step, we apply a forward diffusion process to effectively smooth out the potential perturbations in imperfect demonstrations by introducing additional noise. Subsequently, a reverse generative process is utilized to recover the optimal expert demonstrations from the diffused ones. We provide theoretical evidence supporting our approach, demonstrating that total variance distance between the purified and optimal demonstration distributions can be upper-bounded. The evaluation results on MuJoCo demonstrate the effectiveness of our method from different aspects.

1 Introduction

Reinforcement Learning (RL) [1, 2] has achieved significant success in addressing sequential decision-making problems [3–5]. The core tenet of RL lies in the learning of an optimal policy via rewarding an agent’s actions during its interaction with the environment. The strategic formulation of reward is essential to the recovery of the best policy. However, the intricacy of reward engineering often poses significant challenges in real-world tasks, leading to the failure of RL algorithms occasionally [6, 7]. In response to these challenges, an alternative approach to policy learning is Imitation Learning (IL) [8–10], a learning framework that utilizes expert behaviors to guide agent learning. One fundamental IL approach is Behavioral Cloning (BC) [11, 12], in which the agent observes the action of the expert and learns a policy by directly minimizing the action probability discrepancy via supervised learning. This offline training manner has been proven to suffer from compounding error when the agent executes the policy, leading it to drift to new and dangerous states [13, 14]. In contrast, Generative Adversarial Imitation Learning (GAIL) [15–19] has revealed that imitation learning can be framed as a problem of matching state-action occupancy measures, resulting in a more accurate policy. Based on the framework of Generative Adversarial Nets (GAN) [20], the discriminator in GAIL is introduced to distinguish demonstrations from expert policy and agent policy, yet the agent policy tries its best to generate behaviors that cheat the judgment of the discriminator.

Current imitation learning approaches have shown promising results under the premise that provided expert demonstrations exhibit high-quality performance. Nonetheless, acquiring optimal demonstrations can often be costly in practical real-world applications. In many cases, the demonstrations available are not optimal, leading to the problem of imperfect demonstrations in imitation learning.

Under such a situation, imitation learning algorithms are prone to failure when expert demonstrations are characterized by noise. Hence, the question of how to effectively learn an optimal policy from imperfect demonstrations becomes central to bridging the application gap of imitation learning from simulated environments to real-world tasks. This issue is critical for enhancing the adaptability and effectiveness of imitation learning methods in various practical scenarios.

Confidence-based methods have been shown to be effective when addressing the issue of imperfect demonstrations in imitation learning. In WGAIL [21] and SAIL [22], confidence estimation for each demonstration is tied to the discriminator during the adversarial training phase. BCND [12] proposes that the agent’s policy itself can estimate confidence. Rather than predicting the confidence directly through either policy or discriminator, CAIL [23] considers confidence as a learnable parameter and jointly optimizes it with imitation learning methods. The key of confidence-based methods lies in how to derive proper confidence for each expert demonstration. However, most existing methods integrate confidence estimation into the training of IL [24], leading to a bi-level optimization problem. This bi-level optimization can become unstable and hard to converge during the training of imitation learning, resulting in a breakdown of the confidence estimation. Furthermore, the aforementioned methods are specifically designed to be compatible with either BC or GAIL. This specificity limits their flexibility and restricts their application with other methods.

Rather than integrating the handling of imperfect demonstrations into IL training, we propose an approach where the purification of imperfect demonstrations is performed first. Subsequently, imitation learning is carried out with purified demonstrations. Based on this idea, we introduce Diffusion Purified Imitation Learning (DP-IL), which utilizes the forward and reverse processes in diffusion models to recover the optimal expert demonstrations from imperfect ones. By incorporating the diffusion process into denoising imperfect demonstrations, we provide theoretical analysis on the effectiveness of perturbation elimination during the forward diffusion process as well as the reduction of the gap between the optimal and purified expert distributions. The value gap between the purified and optimal demonstration distributions can also be upper-bounded. We show this strategy is general and can be equipped with both online and offline imitation learning methods. Experimental results in MuJoCo [25] demonstrate the effectiveness of our method from different aspects.

2 Background

Before diving into our method, we briefly review the definition of the Markov Decision Process (MDP) and Imitation Learning with Distribution Matching.

2.1 Markov Decision Process (MDP)

MDP is popular for formulating reinforcement learning (RL) [26] and imitation learning (IL) problems. An MDP normally consists six basic elements $M = (\mathcal{S}, \mathcal{A}, \mathcal{P}, \mathcal{R}, \gamma, \mu_0)$, where \mathcal{S} is a set of states, \mathcal{A} is a set of actions, $\mathcal{P} : \mathcal{S} \times \mathcal{A} \times \mathcal{S} \rightarrow [0, 1]$ is the stochastic transition probability from current state s to the next state s' , $\mathcal{R} : \mathcal{S} \times \mathcal{A} \rightarrow \mathbb{R}$ is the obtained reward of agent when taking action a in a certain state s , $\gamma \in [0, 1]$ is the discounted rate and $\mu_0 : \mathcal{S} \rightarrow [0, 1]$ denotes the initial state distribution.

Definition 1 (Occupancy Measure). *For any policy $\pi(a|s) : \mathcal{S} \rightarrow \mathcal{A}$, there is an one-to-one correspondence between π and its occupancy measure $\rho_\pi : \mathcal{S} \times \mathcal{A} \rightarrow [0, 1]$, which is formulated as*

$$\rho_\pi(s, a) = (1 - \gamma)\pi(a|s) \sum_{t=0}^{\infty} \gamma^t \Pr(s_t = s | \pi), \quad (1)$$

where $\Pr(s_t = s | \pi)$ denotes the probability density of state s at timestep t following policy π .

Definition 2 (Policy Value). *Given the occupancy measure $\rho_\pi(s, a)$, its corresponding policy value (i.e., cumulative rewards with a discount factor $\gamma \in [0, 1]$) is defined to be*

$$V_\pi = \mathbb{E} \left[\sum_{t=0}^{\infty} \gamma^t r(s_t, a_t) \mid s_0 \sim \mu_0, a_t \sim \pi(\cdot|s), s_{t+1} \sim P(\cdot|s_t, a_t), t = 0, 1, 2, \dots \right]. \quad (2)$$

Assuming no loss of generality, we bound the reward function by R_{max} , i.e., $|r(s_t, a_t)| \leq R_{max}, \forall s_t, a_t \in \mathcal{S}, \mathcal{A}$.

2.2 Imitation Learning via Distribution Matching

The field of Imitation Learning (IL) is concerned with optimizing an agent’s behavior in a given environment by utilizing expert demonstrations. Given expert demonstrations \mathcal{D}_e sampled from the expert policy π_e , imitation learning methods aim to let the agent policy π_θ replicate the expert behavior. Distribution Matching (DM) approaches attempt to match the agent’s state-action distribution ρ_{π_θ} with that of the expert’s ρ_{π_e} by minimizing the f -divergence [27, 28],

$$\theta^* = \arg \min_{\theta} D_f(\rho_{\pi_e}, \rho_{\pi_\theta}) = \arg \min_{\theta} \sum_{s,a} \rho_{\pi_\theta}(s,a) f\left(\frac{\rho_{\pi_e}(s,a)}{\rho_{\pi_\theta}(s,a)}\right), \quad (3)$$

where $f : \mathbb{R}^+ \rightarrow \mathbb{R}$ is a convex, lower semi-continuous function and satisfies $f(1) = 0$. Different choices of f -divergence can recover different imitation learning methods. For example, using KL divergence, Jensen-Shannon divergence can recover Behavior Cloning (BC) [12], Generative Adversarial Imitation Learning (GAIL) [15], respectively.

3 Diffusion Purified Imitation Learning

Imitation learning achieves promising results in benchmark tasks with a non-trivial assumption that expert demonstrations should sample from an optimal policy, which may not always hold in practice. In this paper, we consider the problem of imitation-learning-from-imperfect-demonstrations and propose our two-step method *Diffusion Purified Imitation Learning* (DP-IL) to address this problem. In this section, we first illustrate that perturbations in imperfect demonstrations can affect the performance of imitation learning. To mitigate this issue, we add noise to imperfect demonstrations following the forward process of the diffusion model, from which the denoised expert demonstrations are recovered by a reverse-time diffusion process. Furthermore, we provide theoretical results that offer a guarantee for the effectiveness of the proposed method.

3.1 Perturbations in Imperfect Demonstrations

We first formalize the imperfect demonstration problem. For simplicity, we denote the optimal expert state-action distribution as ρ_o where the optimal expert demonstrations are sampled. Due to the high cost of optimal expert demonstration collections, the collected expert demonstrations are always non-optimal in practice. Thus, most accessible expert demonstrations can be imperfect, sampled from a non-optimal expert distribution ρ_n . We argue that the involvement of ρ_n could significantly hurt the optimization of imitation learning algorithms. Specifically, the optimal solution θ^* of the distribution matching in Eq. 3 based on optimal expert distribution can be formulated as $\theta^* = \arg \min_{\theta} D_f(\rho_o, \rho_\theta)$ while the one based on non-optimal expert distribution can be formulated as $\tilde{\theta} = \arg \min_{\theta} D_f(\rho_n, \rho_\theta)$, where $\tilde{\theta}$ denotes a sub-optimal solution. Existing works propose to dynamically adapt the non-optimal expert distribution ρ_n during the training. However, the unstable training in AIL can seriously affect the adaption of ρ_n , resulting in a collapse to imitation learning especially when there exists a high ratio of contamination within \mathcal{D}_n [12]. Thus, to tackle this problem, we first purify the imperfect demonstrations sampled from ρ_n via a distribution transformation and then conduct imitation learning by minimizing the divergence between optimal and purified distributions. Considering a distribution transformation \mathcal{F} , our objective can be formulated as

$$\hat{\theta} = \arg \min_{\theta} D_f(\mathcal{F}^*(\rho_n), \rho_\theta), \quad \text{s.t. } \mathcal{F}^* = \arg \min_{\mathcal{F}} d(\rho_o, \mathcal{F}(\rho_n)), \quad (4)$$

where d denotes the distance measurement between distributions. Note that the imperfect demonstrations mainly come from the potential perturbations δ during the collections, which form the non-optimal expert distribution. Thus, taking \mathcal{F}^* as a denoising function can be a potential solution to tackle the gap between optimal and non-optimal expert distributions. Motivated by the success of diffusion models [29–32], we introduce a Diffusion Purified Imitation Learning (DP-IL) algorithm, which eliminates the potential perturbations δ in ρ_n through a two-step diffusion process. As in the diffusion models, the first step involves a forward diffusion process, where small timestep noise is gradually added to the non-optimal expert demonstrations. This results in diffused demonstrations that eliminate potential perturbation patterns in the non-optimal expert distribution ρ_n while preserving the original semantic information. In the second step, a reverse-time diffusion process is applied to recover the purified demonstrations from the diffused demonstrations.

Algorithm 1 Diffusion Model Training

```

1: repeat
2:   Sample  $x_0 \sim \rho_o(x)$ ,  $i \sim \text{Uniform}(\{0, \dots, T-1\})$ ,  $\epsilon \sim \mathcal{N}(0, I)$  for diffusion training;
3:   Optimize diffusion model  $\phi$  by taking gradient decent step on

$$\nabla_\phi [\epsilon - \phi(\sqrt{\bar{\alpha}_i} \cdot x_0 + \sqrt{1 - \bar{\alpha}_i} \epsilon, i)]^2$$

4: until converged

```

Algorithm 2 Diffusion Purification

```

1: Sample imperfect demonstrations  $x_0$  from  $\rho_{\pi_n}$ ;
2: Calculate  $x_{i^*}$  via forward diffusion:

$$x_{i^*} = \sqrt{\bar{\alpha}_i} \cdot x_0 + \sqrt{1 - \bar{\alpha}_i} \epsilon, \quad \epsilon \sim \mathcal{N}(0, I).$$

3: for  $i = i^*, \dots, 1$  do
4:   Calculate  $x_{i-1}$  via reverse diffusion:

$$x_{i-1} = \frac{1}{\sqrt{\alpha_i}} \left( x_i - \frac{1 - \alpha_i}{\sqrt{1 - \bar{\alpha}_i} \phi(x_i, i)} \right) + \sqrt{\beta_i} z, \quad z \sim \mathcal{N}(0, I)$$

5: end for
6: return  $\hat{x}_0$ 

```

3.2 Purification via Diffusion Process

We formulate \mathcal{F}^* as a two-step purification as in the diffusion model, which includes forward and reverse diffusion processes. For the diffusion model, we adopt widely-used DDPM [33]. For simplicity, we use x to represent the state-action pair (s, a) in Sections 3.2 and 3.3 since we regard it as a whole during the purification process.

Since the transformation \mathcal{F} is a combination of forward and reverse diffusion processes, we train a diffusion model ϕ on optimal demonstrations from ρ_{π_o} first. To simplify the formulation, we concatenate the state-action pair (s, a) to construct the latent variable x for the diffusion model ϕ . Subsequently, we inject noises ϵ on x , where i indicates the number of steps of the Markov procedure in the DDPM¹, which can be viewed as a variable of the level of noise. The goal of the diffusion model is to reverse the diffusion process (*i.e.*, denoise), yielding the learning objective,

$$\min_{\phi} \mathbb{E}_{x_0, \epsilon} [\epsilon - \phi(\sqrt{\bar{\alpha}_i} \cdot x_0 + \sqrt{1 - \bar{\alpha}_i} \epsilon, i)]^2, \quad (5)$$

where t is sampled from a uniform distribution, ϵ is the Gaussian noise sampled from $\mathcal{N}(0, I)$, α_i is defined to be $\alpha_i = 1 - \beta_i$ and $\bar{\alpha}_i$ is defined to be $\bar{\alpha}_i = \prod_{s=1}^i \bar{\alpha}_s$. We summarize the training of the diffusion model in the above Algorithm 1.

After we obtain the trained diffusion model ϕ , we purify imperfect demonstrations x_0 sample from ρ_{π_n} with ϕ . Supposing $i^* \in \{1, \dots, T\}$ is the timestep that is used in the diffusion purification process, the forward diffusion can be given as follows,

$$x_{i^*} = \sqrt{\bar{\alpha}_i} \cdot x_0 + \sqrt{1 - \bar{\alpha}_i} \epsilon, \quad \epsilon \sim \mathcal{N}(0, I). \quad (6)$$

Then, the reverse diffusion process is used to denoise x_{i^*} to \hat{x}_0 from timestep i^* to 0. The reverse diffusion at every step is defined as

$$x_{i-1} = \frac{1}{\sqrt{\alpha_i}} \left(x_i - \frac{1 - \alpha_i}{\sqrt{1 - \bar{\alpha}_i} \phi(x_i, i)} \right) + \sqrt{\beta_i} z, \quad z \sim \mathcal{N}(0, I). \quad (7)$$

Starting from x_{i^*} , we can recover the \hat{x}_0 from Eq. 7. The process of purifying imperfect demonstrations is summarized in Algorithm 2.

3.3 Purification of Imperfect Demonstrations

We propose to utilize a two-step purification to tackle the potential perturbations in expert demonstrations. We further provide a more theoretical analysis of the effectiveness of our proposed DP-IL in

¹In the analysis presented in the paper, $t \in [0, 1]$ denotes the timestep in VP-SDE, which is a continuous value. We use DDPM, which is a discretization of VP-SDE [34], as the implementation of the diffusion model. The step i in DDPM is a discrete value that varies from 0 to T-1.

imperfect demonstrations. We first analyze the purification effectiveness during the forward diffusion process. Considering the optimal expert distribution ρ_o and the non-optimal one ρ_n , we show that the gap between the diffused distribution $\rho_{o,t}$ and $\rho_{n,t}$ becomes smaller with increasing timestep t , which implies that the potential perturbations can be smoothed via the gradually added noises during the forward process.

Theorem 1. *Let $\{x_t\}_{t \in \{0,1\}}$ be the forward diffusion process in Eq. 6. If we denote $\rho_{o,t}(x)$ and $\rho_{n,t}(x)$ as the respective distributions of x_t when $x_0 \sim \rho_{o,t=0}(x)$ (i.e., optimal demonstration distribution) and $x_0 \sim \rho_{n,t=0}(x)$ (i.e., imperfect demonstration distribution), we then have,*

$$\varsigma \leq -\frac{1}{2} \int \rho_{o,t}(x) \beta_t \|\nabla_x \log \rho_{o,t}(x) - \nabla_x \log \rho_{n,t}(x)\|_2^2 dx \leq 0. \quad (8)$$

where $\varsigma = \frac{\partial D_{KL}(\rho_{o,t}(x) \parallel \rho_{n,t}(x))}{\partial t}$ denotes the derivative of t to the KL divergence between $\rho_{o,t}(x)$ and $\rho_{n,t}(x)$.

Notice that $\varsigma \leq 0$ indicates that the KL divergence between $\rho_{o,t}(x)$ and $\rho_{n,t}(x)$ monotonically decreases towards $t = 0$ to $t = 1$ during the forward diffusion step. In other words, with a relatively larger t in the forward diffusion process, the divergence between optimal and imperfect expert distributions can be minimized. The Fisher divergence $D_{fisher}(p \parallel q)$ between two data distribution p and q is defined to be $\int p \|\nabla \log p - \nabla \log q\|_2^2$. Therefore, we have $\varsigma \leq D_{fisher}(\rho_{o,t}(x) \parallel \rho_{n,t}(x))$. The equality is only satisfied when $\rho_{o,t}(x) = \rho_{n,t}(x)$.

The monotonic decrease of $D_{KL}(\rho_{o,t}(x) \parallel \rho_{n,t}(x))$ towards t implies that the diffused optimal expert distribution and the non-optimal expert distribution become closer as t increases. Suppose there exists an ϵ such that the difference between the diffused optimal expert distribution and the imperfect expert distribution becomes negligible when $D_{KL}(\rho_{o,t}(x) \parallel \rho_{n,t}(x)) \leq \epsilon$. We can then find a minimum $t^* \in [0, 1]$ to achieve this. Starting from $\rho_{n,t^*}(x)$, we can stochastically recover $\rho_o(x)$ at $t = 0$ through the reverse diffusion process. We further provide theoretical evidence that the Total Variance (TV) distance between recovered expert distribution and optimal one can be upper bounded via the two-step purification.

Theorem 2. *Supposing $\rho_{\hat{\pi}_o}(x)$ is the purified demonstration distribution and the score function satisfies that $|s_w(x, t)| \leq \frac{1}{2} C_{s_w}$. The Total Variance distance between $\rho_{\hat{\pi}_o}(x)$ and $\rho_{\pi_o}(x)$ satisfies that with a probability of at least $1 - \varpi$,*

$$D_{TV}(\rho_{\pi_o}(x), \rho_{\hat{\pi}_o}(x)) \leq L(|\delta| + \sqrt{e^{2\zeta(t^*)} - 1} C_{\varpi} + \zeta(t^*) C_{s_w}) + C, \quad (9)$$

where $\zeta(t^*) = \int_0^{t^*} \frac{1}{2} \beta(s_w) ds_w$ and the constant $C_{\varpi} = \sqrt{2d + 4\sqrt{d \log \frac{1}{\varpi}} + 4 \log \frac{1}{\varpi}}$.

As shown in Eq. 9, the TV distance between the optimal expert distribution ρ_{π_o} and the purified expert distribution $\rho_{\hat{\pi}_o}$ can be upper bounded by the terms related to the optimal timestep t^* . Thus, the key hyperparameter during the diffusion purification lies in the timestep t in Eqs. 6 and 7 since there is a trade-off between the perturbation purification and semantic information reservation. According to Theorem 1, t should be set to a relatively large value to guarantee that the potential perturbations are removed in diffused distributions, however, t cannot be arbitrarily large since the semantic information should be maintained.

Theorem 2 shows that $\zeta(t^*)$ monotonically increase with t^* , which makes the upper bound of $D_{TV}(\rho_{\pi_o}(x), \rho_{\hat{\pi}_o}(x))$ monotonically increase with t^* . Note that the objective is to minimize the difference between the policy values between optimal and purified demonstration distributions. Thus, a relatively small t^* is required to achieve a smaller upper bound to satisfy the minimum policy values gap. Together with the analysis in Theorem 1, there exists a trade-off on t between perturbation purification and recovery performance. Some optimal t^* are expected to meet the requirements that the potential perturbation can be eliminated in diffused distribution while the semantic information can also be well maintained for recovery. Intuitively, the minimized gap between ρ_{π_o} and $\rho_{\hat{\pi}_o}$ could benefit the distribution matching in Eq. 4 since the potential perturbations in imperfect demonstrations are smoothed. We further provide theoretical evidence that the involvement of purification can contribute to minimizing the policy value gap.

Theorem 3. *For the purified demonstration distribution $\rho_{\hat{\pi}_o}(x)$ and clean demonstration distribution $\rho_{\pi_o}(x)$, we bound their policy value gap as follows,*

$$R_{\pi_o} - V_{\hat{\pi}_o} \leq \frac{R_{max}}{(1 - \gamma)^2} [L(|\delta| + \sqrt{e^{2\zeta(t^*)} - 1} C_{\varpi} + \zeta(t^*) C_{s_w}) + C], \quad (10)$$

where R_{max} denotes the upper bound of $r(x)$ for $\forall x$ and γ is the discounted rate.

The policy value gap can be upper-bounded via the proposed two-step purification, as shown in Eq. 10, which demonstrates the effectiveness of DP-IL. Similarly, the timestep t^* plays an important role in the upper bound. Thus, tuning timestep t^* is an important hyper-parameter in our experiments.

3.4 Learning from Purified Demonstrations

In Eq. 4, $\mathcal{F}^*(\cdot)$ serves to transform the imperfect expert distribution to an optimal one through a combination of forward and reverse diffusion processes, as outlined in Sections 4.2 and 4.3. Once this transformation is obtained, the agent’s policy can be learned by optimizing Eq. 4. However, since the objective function in Eq. 4 is general and lacks a specific function f , it is necessary to recover the objective function of imitation learning in order to enable agent learning.

For two expert distributions ρ_{π_θ} and $\mathcal{F}^*(\rho_{\pi_n})$, the variational lower bound of their f -divergence can be written as,

$$D_f(\rho_{\pi_\theta}, \mathcal{F}^*(\rho_{\pi_n})) \geq \sup_{\phi} \left(\mathbb{E}_{(s,a) \sim \mathcal{F}^*(\rho_{\pi_n})} [\phi(s,a)] - \mathbb{E}_{(s,a) \sim \rho_{\pi_\theta}} [f^*(\phi(s,a))] \right), \quad (11)$$

where $\phi : (s,a) \rightarrow \text{dom}_{f^*}$ is a function approximator which we refer to as an estimator. We parameterize $\phi(s,a) = h_f(V_w(s,a))$ where V_w is an unconstrained discriminator and h_f is an activation function. Combining with Eq. 11, we can further re-write Eq. 4 as,

$$\hat{\theta} = \arg \min_{\theta} \max_w \mathbb{E}_{(s,a) \sim \mathcal{F}^*(\rho_{\pi_n})} [h_f(V_w(s,a))] - \mathbb{E}_{(s,a) \sim \rho_{\pi_\theta}} [f^*(h_f(V_w(s,a)))]. \quad (12)$$

By defining different f functions and their related activation functions h_f , we can recover different imitation learning methods. To recover offline imitation learning, the f function is defined as $f(u) = u \log u$, and h_f is defined as v . For online imitation learning, f is defined as $f(u) = -(u+1) \log \frac{1+u}{2} + u \log u$, and its corresponding activation function is $h_f(v) = -\log(1+\exp(-v)) + \log 2$.

After $\mathcal{F}^*(\cdot)$ is obtained, we intend to specify the training objective of DP-GAIL and DP-BC.

Starting from the variational imitation learning Eq. 11 in the paper, we define the objective function of \mathcal{J} as

$$\mathcal{J}(\theta, w) = \mathbb{E}_{(s,a) \sim \mathcal{F}^*(\rho_{\pi_n})} [h_f(V_w(s,a))] - \mathbb{E}_{(s,a) \sim \rho_{\pi_\theta}} [f^*(h_f(V_w(s,a)))]. \quad (13)$$

By defining f as $f(u) = -(u+1) \log \frac{1+u}{2} + u \log u$ and its corresponding activation function as $h_f(v) = -\log(1+\exp(-v)) + \log 2$, we can see the DP-GAIL objective as,

$$\min_{\theta} \max_w \mathbb{E}_{(s,a) \sim \mathcal{F}^*(\rho_{\pi_n})} [\log D_w(s,a)] + \mathbb{E}_{(s,a) \sim \rho_{\pi_\theta}} [\log(1 - D_w(s,a))], \quad (14)$$

where we choose the last nonlinearity in the discriminator $D_w(s,a)$ as the sigmoid $D_w(s,a) = 1/(1 + e^{-V_w(s,a)})$.

The objective function for DP-BC is deferred to the appendix due to space limitations. In the experiments, DP-BC and DP-GAIL are used as our methods.

4 Experiments

In this section, we conduct extensive experiments to verify the effectiveness of our proposed method Diffusion Purified Imitation Learning in MuJoCo [25] with different imitation learning baselines. The experimental results demonstrate the advantage of DP-IL from different aspects.

Experimental Setting We conduct experiments on four MuJoCo [25] tasks (*i.e.*, Ant-v2, HalfCheetah-v2, Walker2d-v2 and Hopper-v2) in OpenAI Gym [35]. The evaluated performance in MuJoCo can be measured by both the average cumulative ground-truth rewards and the final location of the agent (*i.e.*, the higher the better). We repeat experiments for 5 trials with different random seeds for common practice.

Compared Methods The purified demonstrations are applied to both the offline imitation learning method (*e.g.*, BC) and the online imitation learning method (*e.g.*, GAIL), to demonstrate the effectiveness of the DP-IL. In the case of offline imitation learning, we compare our method DP-BC against

Table 1: Performance of proposed method and other compared offline imitation learning methods in 4 MuJoCo tasks with demonstrations of varying quality. The performance is measured by the average of ground-truth cumulative reward along 10 trajectories (*i.e.*, higher average value is better). The value in the bracket denotes the growth multiplier compared to the best-compared method.

Task	Data	BC-opt	BC-all	BCND [12]	DWBC [36]	D-REX [37]	DP-BC(Ours)
Ant	D1	29	-22	28	-53	-2017	261 ($\uparrow 9.0 \times$)
	D2	29	292	199	-273	-2256	803 ($\uparrow 2.8 \times$)
	D3	29	1500	1951	-152	-2355	2547 ($\uparrow 1.3 \times$)
	Mixed	29	193	411	-335	-1863	601 ($\uparrow 1.5 \times$)
HalfCheetah	D1	-254	1262	1267	-40	709	1365 ($\uparrow 1.1 \times$)
	D2	-254	1264	1862	26	1232	2440 ($\uparrow 1.3 \times$)
	D3	-254	859	834	29	1413	4042 ($\uparrow 2.9 \times$)
	Mixed	-254	1255	921	-198	1036	3146 ($\uparrow 2.5 \times$)
Walker2d	D1	-4	21	102	351	450	1697 ($\uparrow 3.8 \times$)
	D2	-4	1551	1635	297	295	1722 ($\uparrow 1.1 \times$)
	D3	-4	815	192	554	258	3020 ($\uparrow 3.7 \times$)
	Mixed	-4	169	441	232	433	1390 ($\uparrow 3.2 \times$)
Hopper	D1	320	743	590	268	72	1000 ($\uparrow 1.3 \times$)
	D2	320	2044	2119	382	49	3145 ($\uparrow 1.5 \times$)
	D3	320	3090	2883	406	45	3825 ($\uparrow 1.2 \times$)
	Mixed	320	587	564	336	52	655 ($\uparrow 1.1 \times$)

several state-of-the-art methods, including BCND [12], DWBC [36], as well as preference-based methods such as D-REX [37]. For online imitation learning, we compare DP-GAIL with several state-of-the-art confidence-based methods, including 2IWIL [38], IC-GAIL [38], and WGAIL [21].

Source of Imperfect Demonstrations We collect imperfect demonstrations with varying levels of optimality to conduct experiments. First, we trained an optimal expert policy, denoted as π_o , using the Trust Region Policy Optimization (TRPO) algorithm [39]. Then, we collect imperfect demonstrations \mathcal{D}_n by adding Gaussian noise δ into the optimal action distribution $a^* \sim \pi_o$ during the sampling process. Specifically, the action is modeled as $a \sim \mathcal{N}(a^*, \delta^2)$ and we choose $\delta = [0.6, 0.4, 0.25]$ to obtain three different datasets of imperfect demonstrations of varying quality, denoted as D1, D2, and D3 demonstrations. We also investigate how different types of imperfect demonstrations affect the performance of DP-IL, as illustrated in Section 5.2. In addition, since we use a small fraction of optimal demonstrations \mathcal{D}_o (less than 10%) to train the diffusion model, we also include \mathcal{D}_o into the training for a fair comparison. Further details (*e.g.*, implementation of DP-IL and compared methods, data quality, etc.) and more results can be found in the supplementary material.

4.1 Imitation Performance

Purified Offline Imitation Learning We evaluated the effectiveness of our purified imitation learning approach when combined with the offline imitation learning method BC. The results are presented in Table 1. BC-opt means we only use \mathcal{D}_o to conduct BC training, while BC-all means we use both \mathcal{D}_o and \mathcal{D}_n to train the policy network. Our findings align with those reported in [40], showing that using only \mathcal{D}_o can sometimes yield worse performance compared to BC-all. This can be attributed to the insufficient coverage of the entire optimal demonstration space by a limited number of optimal demonstrations. BC-all benefits from a larger training dataset and can outperform BC-opt in certain cases. However, the challenge of imperfect demonstrations still hampers BC’s ability to achieve optimal performance. In contrast, our proposed method focuses on purifying the imperfect demonstrations before training, consistently improving the performance of behavior cloning across all D1, D2, and D3 demonstrations compared to its baseline and other comparison methods. This demonstrates the efficacy of our approach in enhancing the performance of behavior cloning by addressing the limitations posed by imperfect demonstrations.

Mixed Demonstrations In addition to collecting imperfect demonstrations from a single demonstrator, we also investigate the performance of DP-IL when confronted with imperfect demonstrations that are a mixture of non-optimal demonstrations. The results are presented in Table 1, where the term “Mixed” demonstrations denote a combination of D1, D2, and D3 demonstrations. As shown in

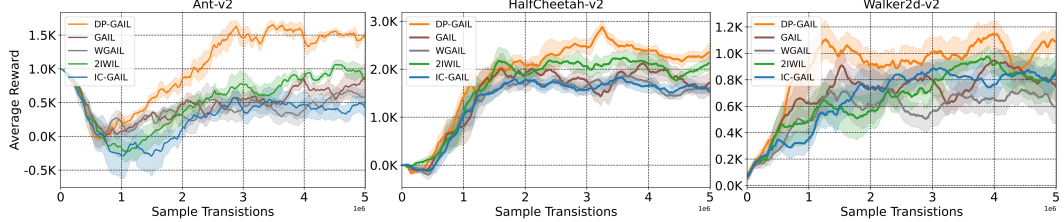


Figure 1: The training curve of DP-GAIL and other online imitation learning methods in 3 MuJoCo tasks with D1 demonstrations. The x-axis is the number of interactions with the environment and the shaded area indicates the standard error.

Table 2: MMD distance evaluation.

Task	D1	D2	D3
$MMD(\rho_{\pi_o}, \rho_{\pi_n})$	0.210	0.146	0.078
$MMD(\rho_{\pi_o}, \rho_{\hat{\pi}_o})$	0.198	0.139	0.074

Table 3: The p-value between DP-GAIL and the baseline GAIL.

Task	Ant	HalfCheetah	Walker2d
p-value	0.031	0.061	0.026

the table, DP-BC with mixed demonstrations also consistently outperforms the baseline and other compared methods by a substantial margin. Specifically, the average reward of DP-BC is $3.1 \times$, $2.5 \times$, $8.2 \times$, and $1.1 \times$ higher than the baseline in Ant, HalfCheetah, Walker2d, and Hopper, respectively. Hence, we conclude that our proposed method Diffusion Purified Imitation Learning is able to deal with imperfect demonstrations from multiple demonstrators.

Purified Online Imitation Learning Besides offline imitation learning, we also utilize diffusion-purified demonstrations for GAIL training and compare DP-GAIL with other *state-of-the-art* online imitation learning methods that also address the imperfect demonstration issue. The training curves of DP-GAIL and other compared methods are depicted in Figure 1. The curve unequivocally demonstrates the superiority of DP-GAIL over other compared methods. This shows the efficacy of noise purification in improving the performance of online imitation learning methods. Moreover, we conducted a student’s t-test on the results, where the null hypothesis is that the performance of DP-GAIL is similar to or worse than the GAIL baseline. The results, shown in Table 3, indicate that there is a statistically significant difference between the performance of DP-GAIL and the baseline GAIL since most p-values are only around 0.05 in the four tasks.

Effectiveness of Purification In Theorem 2, we provide theoretical evidence that the gap between optimal expert demonstration distribution ρ_{π_o} and purified demonstration distribution $\rho_{\hat{\pi}_o}$ can be upper bounded. We further provide empirical evidence that the purification can be successfully achieved. We conduct experiments to measure the Maximum Mean Discrepancy (MMD) distance between optimal demonstrations and imperfect demonstrations as well as the one between optimal demonstrations and purified demonstrations. We sample 500 demonstrations from these distributions for MMD computation. The results are shown in Table 2. The MMD distances between ρ_{π_o} and ρ_{π_o} are 0.074, 0.139, and 0.198, while the MMD distance between ρ_{π_o} and ρ_{π_n} are 0.078, 0.146, and 0.210 with D1, D2 and D3 demonstrations respectively in HalfCheetah-v2 task. The results demonstrate that the purified expert distribution always have a closer gap with the optimal one than the non-optimal one under various settings. We mainly attribute it to the upper bound with the involvement of purification. Thus, the MMD reduction strongly supports the Theorem 2 and the effectiveness of our proposed purification.

4.2 Ablation Study

Impact of optimal t^* As discussed in Section 4.3, $t^* \in [0, 1]$ is an important hyper-parameter to achieve the trade-off between smoothing the noise and keeping semantic information. To investigate how the choice of t^* affects the effectiveness of noise purification, we conducted experiments on demonstrations with different levels of optimality. Our empirical results confirmed the theoretical findings of Theorem 1, suggesting that demonstrations with less optimality require a relatively larger timestep t^* to smooth the noise. For example, in Ant-v2 task, the optimal t^* is 0.1 for D1 demonstrations while the optimal t^* is 0.01 for D3 demonstrations. As the quality of demonstrations improved (e.g., from D1 to D3), we observed a gradual decrease in the optimal value of t^* . This

Table 4: Performance of proposed methods and compared methods in MuJoCo tasks with demonstrations from early checkpoint during the RL training. The value in brackets (\cdot) denotes the optimal t^* for DP-BC to achieve the best performance.

Method	D4			D5		
	Ant	HalfCheetah	Walker2d	Ant	HalfCheetah	Walker2d
BC-all	1089	1314	501	1356	1780	2702
BCND [12]	1539	1498	686	2232	1990	2574
DP-BC(t^*)	1572(0.03)	1530(0.03)	2208(0.03)	3414(0.005)	4748(0.01)	3076(0.005)

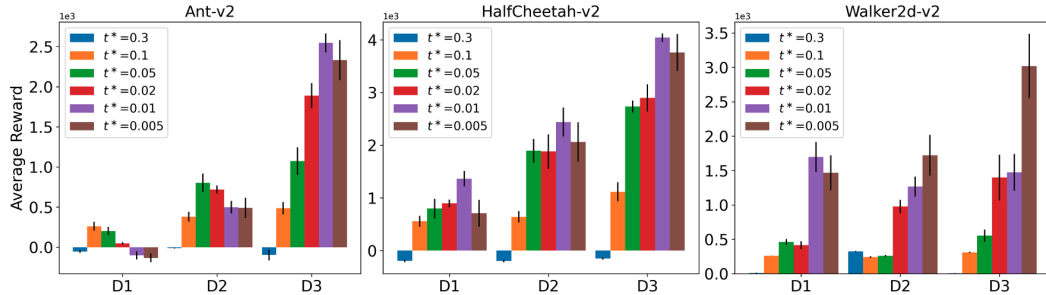


Figure 2: Impact of diffusion time t^* with demonstrations of different optimality. We report the performance of DP-BC here and the dotted line indicates the performance of BC baseline.

could lead to a smaller value bound since $\zeta(t^*)$ exhibits a monotonic increase with respect to t^* . Hence, diffusion purified imitation learning should perform better when using a smaller t^* under such a case, which is consistent with the results in Figure 2.

Different Types of Imperfect Demonstrations For D1, D2 and D3 demonstrations, we formulate them by introducing different noises into the optimal policy’s action during the sampling process. Besides, we also examined the performance of DP-IL with a different type of imperfect demonstration. Typically, sampling demonstrations from the early checkpoint during the RL training has also been widely used to formulate imperfect demonstrations [38]. Therefore, we collected two checkpoints during the training of π_o and obtained two types of imperfect demonstrations (e.g., D4 and D5 demonstrations), where the latter are of higher quality. We compared DP-BC with BC, and the results are presented in Table 4. As evident from the table, DP-BC outperformed the baseline and the compared method in all three tasks and both kinds of demonstrations, demonstrating the generalization ability of DP-BC when dealing with different types of imperfect data. We also observed that the optimal t^* followed similar patterns to this type of imperfect demonstration, where highly imperfect data required a larger t^* .

Compared with Other Purified Methods

The transformation $\mathcal{F}(\cdot)$ is defined as a combination of the forward and reverse diffusion processes to denoise imperfect demonstrations. Apart from the diffusion model, there are various denoising methods that can be employed as the transformation \mathcal{F}^* . Since filters are commonly used to smooth noisy data,

we utilize three different filters (mean, median, and Gaussian) as \mathcal{F}^* to denoise the imperfect demonstrations. The results are presented in Table 5. It is evident from the table that our method outperforms other filter-based methods in all types of imperfect demonstrations (e.g., D1, D2, and D3). Among the filter-based methods, the ‘Mean Filter’ achieves the best performance. Another notable finding is that when the noise level is high in imperfect demonstrations (e.g., D1 demonstrations), filter-based methods tend to maintain a greater advantage over the baseline.

Table 5: The performance of DP-IL on Ant-v2 task when defining different \mathcal{F}^* in Eq. 4. ‘G-Filter’, ‘Mean-Filter’ and ‘Med-Filter’ denote using Gaussian, Mean and Median Filter as \mathcal{F}^* to denoise imperfect demonstrations.

	BC	DP-BC	G-Filter	Mean-Filter	Med-Filter
D1	-22	261	242	182	138
D2	292	803	729	736	437
D3	1500	2547	771	1786	455

5 Related Work

In imitation learning, confidence-based methods estimate the weight for each demonstration to address its importance to agent learning. 2IWIL [38] and IC-GAIL [38] first investigate the effectiveness of weighting schemes in imitation learning with imperfect demonstrations. However, these approaches relied on manually labeled confidence, which is challenging to obtain in practical scenarios. To relax this requirement, subsequent works have proposed alternative methods. For instance, DWBC [36] and DICE-based methods [40–42] leverage a small fraction of known optimal demonstrations to infer the weights for the remaining supplementary demonstrations. CAIL [23] utilizes partially ranked trajectories to guide confidence estimation. Recent works also focus on estimating confidence without prior information. WGAIL [21] and SAIL [22] connect confidence to the discriminator during training. BCND [12] use the policy network to indicate confidence. However, these approaches have two primary limitations. First, the weight estimation and imitation learning build up a bi-level optimization problem, which can be challenging to converge. Secondly, most methods rely on having a certain proportion of optimal demonstrations, which may not be feasible in practical settings.

Preference-based methods [43, 44] have proven effective for policy learning. Using human preference can avoid complex reward engineering, thus making policy learning more practical. T-REX [45] focuses on extrapolating a reward function based on ranked trajectories. By effectively capturing the rankings, the learned reward function provides valuable feedback to guide the agent’s learning process. T-REX only requires precise rankings of trajectories, yet does not set constraints on data quality. As a result, T-REX can achieve satisfactory performance even in scenarios where optimal trajectories are unavailable. D-REX [37] introduces relaxation to the ranking constraint of T-REX. Initially, it learns a pre-trained policy through behavioral cloning and subsequently generates ranked trajectories by injecting varying levels of noise into the actions. D-REX uses the same way to learn the reward as T-REX with ranked trajectories. To address potential ranking errors, SSRR [46] proposes a novel reward function structure. By mitigating the adverse effects arising from ranking inaccuracies, SSRR enhances the reliability of the learning process.

6 Conclusion

In this paper, we propose to tackle the imperfect expert demonstration issue from a perspective of perturbation. We conduct a two-step purification process to eliminate the potential perturbations based on the diffusion process before conducting imitation learning. The distance gap between optimal and imperfect expert distributions can be minimized after forward diffusion. The purified expert distribution can be recovered from diffused one via reverse diffusion. We provide sufficient theoretical analysis that the proposed two-step purification can eliminate the potential perturbations and minimize the divergence between optimal and purified expert distributions. With purified expert demonstrations, the subsequent distribution matching in imitation learning can be more accurate to improve agent behavior. Our proposed DP-IL algorithms can be easily adopted in existing imitation learning frameworks, such as GAIL and BC, to alleviate the imperfect expert demonstrations at any ratios. We conduct extensive experiments on different tasks and apply the proposed DP-IL on different IL algorithms to evaluate the effectiveness with imperfect demonstrations. The comparison results demonstrate the superiority of DP-IL over other baselines.

References

- [1] Richard S Sutton and Andrew G Barto. *Reinforcement learning: An introduction*. MIT press, 2018.
- [2] Leslie Pack Kaelbling, Michael L Littman, and Andrew W Moore. Reinforcement learning: A survey. *Journal of artificial intelligence research*, 4:237–285, 1996.
- [3] David Silver, Aja Huang, Chris J Maddison, Arthur Guez, Laurent Sifre, George Van Den Driessche, Julian Schrittwieser, Ioannis Antonoglou, Veda Panneershelvam, Marc Lanctot, et al. Mastering the game of go with deep neural networks and tree search. *nature*, 529(7587):484–489, 2016.
- [4] Hado Van Hasselt, Arthur Guez, and David Silver. Deep reinforcement learning with double q-learning. In *Proceedings of the AAAI conference on artificial intelligence*, volume 30, 2016.

[5] Daochen Zha, Jingru Xie, Wenye Ma, Sheng Zhang, Xiangru Lian, Xia Hu, and Ji Liu. Douzero: Mastering doudizhu with self-play deep reinforcement learning. In *International Conference on Machine Learning*, pages 12333–12344. PMLR, 2021.

[6] Dario Amodei, Chris Olah, Jacob Steinhardt, Paul Christiano, John Schulman, and Dan Mané. Concrete problems in ai safety. *arXiv preprint arXiv:1606.06565*, 2016.

[7] Gabriel Dulac-Arnold, Daniel Mankowitz, and Todd Hester. Challenges of real-world reinforcement learning. *arXiv preprint arXiv:1904.12901*, 2019.

[8] Pieter Abbeel and Andrew Y Ng. Apprenticeship learning via inverse reinforcement learning. In *Proceedings of the twenty-first international conference on Machine learning*, page 1. ACM, 2004.

[9] Ahmed Hussein, Mohamed Medhat Gaber, Eyad Elyan, and Christina Jayne. Imitation learning: A survey of learning methods. *ACM Computing Surveys (CSUR)*, 50(2):1–35, 2017.

[10] Xin-Qiang Cai, Yao-Xiang Ding, Yuan Jiang, and Zhi-Hua Zhou. Imitation learning from pixel-level demonstrations by hashreward. In *Proceedings of the 20th International Conference on Autonomous Agents and MultiAgent Systems*, pages 279–287, 2021.

[11] Faraz Torabi, Garrett Warnell, and Peter Stone. Behavioral cloning from observation. In *Proceedings of the 27th International Joint Conference on Artificial Intelligence*, pages 4950–4957, 2018.

[12] Fumihiro Sasaki and Ryota Yamashina. Behavioral cloning from noisy demonstrations. In *International Conference on Learning Representations*, 2021.

[13] Tian Xu, Ziniu Li, and Yang Yu. Error bounds of imitating policies and environments. *Advances in Neural Information Processing Systems*, 33:15737–15749, 2020.

[14] Tian Xu, Ziniu Li, and Yang Yu. Error bounds of imitating policies and environments for reinforcement learning. *IEEE Transactions on Pattern Analysis and Machine Intelligence*, 44(10):6968–6980, 2021.

[15] Jonathan Ho and Stefano Ermon. Generative adversarial imitation learning. In *Advances in neural information processing systems*, pages 4565–4573, 2016.

[16] Justin Fu, Katie Luo, and Sergey Levine. Learning robust rewards with adversarial inverse reinforcement learning. *arXiv preprint arXiv:1710.11248*, 2017.

[17] Robert Dadashi, Leonard Hussenot, Matthieu Geist, and Olivier Pietquin. Primal wasserstein imitation learning. In *International Conference on Learning Representations*, 2020.

[18] Xin-Qiang Cai, Yao-Xiang Ding, Zi-Xuan Chen, Yuan Jiang, Masashi Sugiyama, and Zhi-Hua Zhou. Seeing differently, acting similarly: Heterogeneously observable imitation learning. *arXiv preprint arXiv:2106.09256*, 2021.

[19] Yunke Wang, Bo Du, and Chang Xu. Unlabeled imperfect demonstrations in adversarial imitation learning. *arXiv preprint arXiv:2302.06271*, 2023.

[20] Ian Goodfellow, Jean Pouget-Abadie, Mehdi Mirza, Bing Xu, David Warde-Farley, Sherjil Ozair, Aaron Courville, and Yoshua Bengio. Generative adversarial nets. In *Advances in neural information processing systems*, pages 2672–2680, 2014.

[21] Yunke Wang, Chang Xu, Bo Du, and Honglak Lee. Learning to weight imperfect demonstrations. In *International Conference on Machine Learning*, pages 10961–10970. PMLR, 2021.

[22] Yunke Wang, Chang Xu, and Bo Du. Robust adversarial imitation learning via adaptively-selected demonstrations. In *Proceedings of the Thirtieth International Joint Conference on Artificial Intelligence*, pages 3155–3161, 2021.

[23] Songyuan Zhang, Zhangjie Cao, Dorsa Sadigh, and Yanan Sui. Confidence-aware imitation learning from demonstrations with varying optimality. *Advances in Neural Information Processing Systems*, 34:12340–12350, 2021.

[24] Mark Beliaev, Andy Shih, Stefano Ermon, Dorsa Sadigh, and Ramtin Pedarsani. Imitation learning by estimating expertise of demonstrators. In *International Conference on Machine Learning*, pages 1732–1748. PMLR, 2022.

[25] Emanuel Todorov, Tom Erez, and Yuval Tassa. Mujoco: A physics engine for model-based control. In *2012 IEEE/RSJ International Conference on Intelligent Robots and Systems*, pages 5026–5033. IEEE, 2012.

[26] Martin L. Puterman. *Markov Decision Processes: Discrete Stochastic Dynamic Programming*. Wiley Series in Probability and Statistics. Wiley, 1994.

[27] Sebastian Nowozin, Botond Cseke, and Ryota Tomioka. f-gan: Training generative neural samplers using variational divergence minimization. *Advances in neural information processing systems*, 29, 2016.

[28] Liyiming Ke, Matt Barnes, Wen Sun, Gilwoo Lee, Sanjiban Choudhury, and Siddhartha Srinivasa. Imitation learning as f -divergence minimization. *arXiv preprint arXiv:1905.12888*, 2019.

[29] Ling Yang, Zhilong Zhang, Yang Song, Shenda Hong, Runsheng Xu, Yue Zhao, Yingxia Shao, Wentao Zhang, Bin Cui, and Ming-Hsuan Yang. Diffusion models: A comprehensive survey of methods and applications. *arXiv preprint arXiv:2209.00796*, 2022.

[30] Yunke Wang, Xiyu Wang, Anh-Dung Dinh, Bo Du, and Charles Xu. Learning to schedule in diffusion probabilistic models. In *Proceedings of the 29th ACM SIGKDD Conference on Knowledge Discovery and Data Mining*, pages 2478–2488, 2023.

[31] Weili Nie, Brandon Guo, Yujia Huang, Chaowei Xiao, Arash Vahdat, and Anima Anandkumar. Diffusion models for adversarial purification. *arXiv preprint arXiv:2205.07460*, 2022.

[32] Xizewen Han, Huangjie Zheng, and Mingyuan Zhou. Card: Classification and regression diffusion models. *Advances in Neural Information Processing Systems*, 35:18100–18115, 2022.

[33] Jonathan Ho, Ajay Jain, and Pieter Abbeel. Denoising diffusion probabilistic models. *Advances in Neural Information Processing Systems*, 33:6840–6851, 2020.

[34] Yang Song, Jascha Sohl-Dickstein, Diederik P Kingma, Abhishek Kumar, Stefano Ermon, and Ben Poole. Score-based generative modeling through stochastic differential equations. *arXiv preprint arXiv:2011.13456*, 2020.

[35] Greg Brockman, Vicki Cheung, Ludwig Pettersson, Jonas Schneider, John Schulman, Jie Tang, and Wojciech Zaremba. Openai gym, 2016.

[36] Haoran Xu, Xianyuan Zhan, Honglei Yin, and Huiling Qin. Discriminator-weighted offline imitation learning from suboptimal demonstrations. In *International Conference on Machine Learning*, pages 24725–24742. PMLR, 2022.

[37] Daniel S Brown, Wonjoon Goo, and Scott Niekum. Better-than-demonstrator imitation learning via automatically-ranked demonstrations. In *Conference on Robot Learning*, pages 330–359, 2020.

[38] Yueh-Hua Wu, Nontawat Charoenphakdee, Han Bao, Voot Tangkaratt, and Masashi Sugiyama. Imitation learning from imperfect demonstration. *arXiv preprint arXiv:1901.09387*, 2019.

[39] John Schulman, Sergey Levine, Pieter Abbeel, Michael Jordan, and Philipp Moritz. Trust region policy optimization. In *International conference on machine learning*, pages 1889–1897, 2015.

[40] Geon-Hyeong Kim, Seokin Seo, Jongmin Lee, Wonseok Jeon, HyeongJoo Hwang, Hongseok Yang, and Kee-Eung Kim. Demodice: Offline imitation learning with supplementary imperfect demonstrations. In *International Conference on Learning Representations*, 2021.

[41] Lantao Yu, Tianhe Yu, Jiaming Song, Willie Neiswanger, and Stefano Ermon. Offline imitation learning with suboptimal demonstrations via relaxed distribution matching. *arXiv preprint arXiv:2303.02569*, 2023.

- [42] Ziniu Li, Tian Xu, Yang Yu, and Zhi-Quan Luo. Theoretical analysis of offline imitation with supplementary dataset. *arXiv preprint arXiv:2301.11687*, 2023.
- [43] Paul F Christiano, Jan Leike, Tom Brown, Miljan Martic, Shane Legg, and Dario Amodei. Deep reinforcement learning from human preferences. In *Advances in Neural Information Processing Systems*, pages 4299–4307, 2017.
- [44] Borja Ibarz, Jan Leike, Tobias Pohlen, Geoffrey Irving, Shane Legg, and Dario Amodei. Reward learning from human preferences and demonstrations in atari. *Advances in neural information processing systems*, 31, 2018.
- [45] Daniel S Brown, Wonjoon Goo, Prabhat Nagarajan, and Scott Niekum. Extrapolating beyond suboptimal demonstrations via inverse reinforcement learning from observations. *arXiv preprint arXiv:1904.06387*, 2019.
- [46] Letian Chen, Rohan Paleja, and Matthew Gombolay. Learning from suboptimal demonstration via self-supervised reward regression. In *Conference on Robot Learning*, pages 1262–1277. PMLR, 2021.
- [47] Yang Song, Conor Durkan, Iain Murray, and Stefano Ermon. Maximum likelihood training of score-based diffusion models. *Advances in Neural Information Processing Systems*, 34:1415–1428, 2021.
- [48] Simo Särkkä and Arno Solin. *Applied stochastic differential equations*, volume 10. Cambridge University Press, 2019.
- [49] Voot Tangkaratt, Bo Han, Mohammad Emtiyaz Khan, and Masashi Sugiyama. Vild: Variational imitation learning with diverse-quality demonstrations. *arXiv preprint arXiv:1909.06769*, 2019.

A Proof for Theorem 1

Theorem 1. Let $\{x_t\}_{t \in \{0,1\}}$ be the forward diffusion process in Eq. 5. If we denote $\rho_{o,t}(x)$ and $\rho_{n,t}(x)$ as the respective distributions of x_t when $x_0 \sim \rho_{o,t=0}(x)$ (i.e., optimal demonstration distribution) and $x_0 \sim \rho_{n,t=0}(x)$ (i.e., imperfect demonstration distribution), we then have,

$$\varsigma \leq -\frac{1}{2} \int \rho_{o,t}(x) \beta_t \|\nabla_x \log \rho_{o,t}(x) - \nabla_x \log \rho_{n,t}(x)\|_2^2 dx \leq 0. \quad (12)$$

where $\varsigma = \frac{\partial D_{KL}(\rho_{o,t}(x) || \rho_{n,t}(x))}{\partial t}$ denotes the derivative of t to the KL divergence between $\rho_{o,t}(x)$ and $\rho_{n,t}(x)$.

Proof. Following the proof in [47], we first make two assumptions on $\rho_{\pi_o,t}(x)$ and $\rho_{\pi_n,t}(x)$. Supposing both $\rho_{\pi_o,t}(x)$ and $\rho_{\pi_n,t}(x)$ are smooth and fast decaying functions, we have

$$\lim_{x \rightarrow \infty} \rho_{\pi_o,t}(x) \frac{\partial}{\partial x} \log \rho_{\pi_o,t}(x) = 0 \quad (13)$$

$$\lim_{x \rightarrow \infty} \rho_{\pi_n,t}(x) \frac{\partial}{\partial x} \log \rho_{\pi_n,t}(x) = 0 \quad (14)$$

The forward diffusion process in Eq. 5 is a discrete Markov chain, which can be written as

$$x_i = \sqrt{1 - \beta_i} \cdot x_{i-1} + \sqrt{\beta_i} \cdot \epsilon, \quad i = 1, \dots, N, \quad (15)$$

where $\epsilon \sim \mathcal{N}(0, I)$. To obtain the limit of this Markov chain when $N \rightarrow \infty$, we define an auxiliary set of noise scales $\{\bar{\beta}_i = N\bar{\beta}_i\}_{i=1}^N$, and re-write Eq. 15 as

$$x_i = \sqrt{1 - \frac{\bar{\beta}_i}{N}} x_{i-1} + \sqrt{\frac{\bar{\beta}_i}{N}} \epsilon, \quad i = 1, \dots, N, \quad (16)$$

In the limit of $N \rightarrow \infty$, $\{\bar{\beta}_i\}_{i=1}^N$ becomes a function β_t indexed by $t \in [0, 1]$. Let $\beta(\frac{i}{N}) = \bar{\beta}_i$, $x(\frac{i}{N}) = x_i$, $\epsilon(\frac{i}{N}) = \epsilon_i$. Hence, we can rewrite Eq. 16 as the following with $\Delta t = \frac{1}{N}$ and $t \in \{0, 1, \dots, \frac{N-1}{N}\}$,

$$x_{t+\Delta t} = \sqrt{1 - \beta_{t+\Delta t} \cdot \Delta t} \cdot x_t + \sqrt{\beta_{t+\Delta t} \cdot \Delta t} \cdot \epsilon_t \quad (17)$$

$$= x_t - \frac{1}{2} \beta_{t+\Delta t} \cdot \Delta t \cdot x_t + \sqrt{\beta_{t+\Delta t}} \cdot \epsilon_t \quad (18)$$

$$= x_t - \frac{1}{2} \beta_t \Delta t \cdot x_t + \sqrt{\beta_t \Delta t} \cdot \epsilon_t. \quad (19)$$

In the limit of $\Delta t \rightarrow 0$, we can transform Eq. 5 to the following VP-SDE,

$$dx = -\frac{1}{2} \beta_t x dt + \sqrt{\beta_t} dw, \quad (20)$$

where w is a standard Wiener process. The Fokker–Planck equation for the VP-SDE above describes the time-evolution of the stochastic process's associated probability density function, and is given by

$$\frac{\partial \rho_{\pi_o,t}(x)}{\partial t} = -\nabla_x \cdot \left(\frac{1}{2} \beta_t \rho_{\pi_o,t}(x) \nabla_x \log \rho_{\pi_o,t}(x) + \frac{1}{2} \beta_t x \rho_{\pi_o,t}(x) \right) \quad (21)$$

$$= -\nabla_x \cdot \left(h_o(x, t) \rho_{\pi_o,t}(x) \right), \quad (22)$$

where $h_o(x, t)$ is defined as $h_o(x, t) = \frac{1}{2}\beta_t \nabla_x \log \rho_{\pi_o, t}(x) + \frac{1}{2}\beta_t x$. Then, we denote $\varsigma = \frac{\partial D_{KL}(\rho_{\pi_o, t}(x) || \rho_{\pi_n, t}(x))}{\partial t}$ and ς can be re-written as follows,

$$\varsigma = \frac{\partial}{\partial t} \int \rho_{\pi_o, t}(x) \log \frac{\rho_{\pi_o, t}(x)}{\rho_{\pi_n, t}(x)} dx \quad (23)$$

$$= \int \frac{\partial \rho_{\pi_o, t}(x)}{\partial t} \log \frac{\rho_{\pi_o, t}(x)}{\rho_{\pi_n, t}(x)} dx + \int \frac{\partial \rho_{\pi_o, t}(x)}{\partial t} dx - \int \frac{\rho_{\pi_o, t}(x)}{\rho_{\pi_n, t}(x)} \frac{\partial \rho_{\pi_n, t}(x)}{\partial t} dx \quad (24)$$

$$= \int \nabla_x \cdot \left(-h_o(x, t) \rho_{\pi_o, t}(x) \right) \log \frac{\rho_{\pi_o, t}(x)}{\rho_{\pi_n, t}(x)} dx - \int \frac{\rho_{\pi_o, t}(x)}{\rho_{\pi_n, t}(x)} \nabla_x \cdot \left(-h_n(x, t) \rho_{\pi_n, t}(x) \right) \quad (25)$$

$$\stackrel{(i)}{=} - \int \rho_{\pi_o, t}(x) [h_o^T(x, t) - h_n^T(x, t)] [\nabla_x \log \rho_{\pi_o, t}(x) - \nabla_x \log \rho_{\pi_n, t}(x)] \quad (26)$$

$$= - \frac{1}{2} \int \rho_{\pi_o, t}(x) \beta_t |\nabla_x \log \rho_{\pi_o, t}(x) - \nabla_x \log \rho_{\pi_o, n}(x)|_2^2 dx, \quad (27)$$

where (i) can be obtained by integration by parts.

B Proof for Theorem 2

Theorem 2. Supposing $\rho_{\hat{\pi}_o}(x)$ is the purified demonstration distribution and the score function satisfies that $|s_w(x, t)| \leq \frac{1}{2}C_{s_w}|$. The Total Variance distance between $\rho_{\hat{\pi}_o}(x)$ and $\rho_{\pi_o}(x)$ satisfies that with a probability of at least $1 - \varpi$,

$$D_{TV}(\rho_{\pi_o}(x), \rho_{\hat{\pi}_o}(x)) \leq L(|\delta| + \sqrt{e^{2\zeta(t^*)} - 1}C_{\varpi} + \zeta(t^*)C_{s_w}) + C, \quad (28)$$

where $\zeta(t^*) = \int_0^{t^*} \frac{1}{2}\beta(s)ds$ and the constant $C_{\varpi} = \sqrt{2d + 4\sqrt{d \log \frac{1}{\varpi}} + 4 \log \frac{1}{\varpi}}$.

Proof. For purified demonstration distribution $\rho_{\hat{\pi}_o}(x)$ and clean demonstration distribution $\rho_{\pi_o}(x)$, their total variance distance can be defined as follows,

$$D_{TV}(\rho_{\pi_o}(x), \rho_{\hat{\pi}_o}(x)) \leq \sum_x |\rho_{\pi_o}(x) - \rho_{\hat{\pi}_o}(x)| \quad (29)$$

$$= \frac{1}{2} \sum_s \left| [\hat{\pi}_o(\cdot|s) - \pi_o(\cdot|s)] d_{\hat{\pi}_o}(s) + [d_{\hat{\pi}_o}(s) - d_{\pi}(s)] \pi_o(\cdot|s) \right| \quad (30)$$

$$\leq \mathbb{E}_{s \sim d_{\hat{\pi}_o}} [D_{TV}(\pi_o(\cdot|s), \hat{\pi}_o(\cdot|s))] + D_{TV}(d_{\pi_o}, d_{\hat{\pi}_o}) \quad (31)$$

$$= \sum_s d_{\hat{\pi}_o}(s) |\pi_o(\cdot|s) - \hat{\pi}_o(\cdot|s)| \quad (32)$$

The stochastic policy is typically modeled via the Gaussian distribution. Therefore, both π_o and $\hat{\pi}_o$ should satisfy the Lipschitz continuity. For $a \sim \pi_o(\cdot|s)$ and $\hat{a} \sim \hat{\pi}_o(\cdot|s)$, there exists a constant L_{π} that can bound $|\pi_o(\cdot|s) - \hat{\pi}_o(\cdot|s)|$ as follow,

$$|\pi_o(a|s) - \hat{\pi}_o(\hat{a}|s)| = |\pi_o(a|s) - \pi_o(\hat{a}|s) + \pi_o(\hat{a}|s) - \hat{\pi}_o(\hat{a}|s)| \quad (33)$$

$$\leq |\pi_o(a|s) - \pi_o(\hat{a}|s)| + |\pi_o(\hat{a}|s) - \hat{\pi}_o(\hat{a}|s)| \quad (34)$$

$$\leq L(a - \hat{a}) + C \quad (35)$$

Eq. 34 can be obtained via triangle inequality and Eq. 35 is due to the Lipschitz continuity. Denote δ is the noise in the imperfect demonstration x and the diffused noise demonstrations x_{t^*} through the forward diffusion process satisfies

$$x_{t^*} = \sqrt{\alpha(t^*)}x + \sqrt{1 - \alpha(t^*)}\epsilon, \quad (36)$$

where $\alpha(t) = \exp - \int_0^t \beta(s) ds$ and $\epsilon \in \mathcal{N}(0, I)$, the L1-distance between the purified demonstrations \hat{x} and its related optimal demonstration x can be bounded as

$$|\hat{x} - x| = |x_{t^*} + (\hat{x} - x_{t^*}) - x| \quad (37)$$

$$= |x_{t^*} + \int_{t^*}^0 -\frac{1}{2} \beta_t [x + 2s_w(x, t)] dt + \int_{t^*}^0 \sqrt{\beta_t} d\bar{w} - x| \quad (38)$$

$$\leq |x_{t^*} + \int_{t^*}^0 -\frac{1}{2} \beta_t x dt + \int_{t^*}^0 \sqrt{\beta_t} d\bar{w} - x| + \left| \int_{t^*}^0 -\beta_t s_w(x, t) dt \right|, \quad (39)$$

where Eq. 38 follows with the definition of reverse-time diffusion and Eq. 39 can be obtained via triangle inequality. The sum of the first 3 terms in Eq. 38 is a time-varying Ornstein-Uhlenbeck process with a negative time increment that starts from $t = t^*$ to $t = 0$ with the initial value set to x_{t^*} . Denote by x'_0 its solution, from [48] we know x'_0 follows a Gaussian distribution, where its mean $\mu(0)$ and covariance matrix $\Sigma(0)$ are the solutions of the following two differential equations, respectively,

$$\frac{d\mu}{dt} = -\frac{1}{2} \beta_t \mu, \quad \frac{d\Sigma}{dt} = \beta_t \Sigma + \beta_t I_d, \quad (40)$$

with the initial conditions $\mu(t^*) = x_{t^*}$ and $\Sigma(t^*) = 0$. By solving these two differential equations, we have that conditioned on x_{t^*} , $x'_0 \sim \mathcal{N}(e^{\zeta(t^*)} x_{t^*}, (e^{2\zeta(t^*)} - 1) I_d)$, where $\zeta(t^*) = \int_0^{t^*} \frac{1}{2} \beta(s) ds$.

Using the reparameterization trick, we have,

$$x'_0 - x = e^{\zeta(t^*)} x_{t^*} + \sqrt{e^{2\zeta(t^*)} - 1} \epsilon_2 - x \quad (41)$$

$$= e^{\zeta(t^*)} \left(e^{-\zeta(t^*)} (x + \delta) + \sqrt{1 - e^{-2\zeta(t^*)}} \epsilon_1 + \sqrt{e^{2\zeta(t^*)} - 1} \epsilon_2 - x \right) \quad (42)$$

$$= \sqrt{e^{2\zeta(t^*)} - 1} (\epsilon_1 + \epsilon_2) + \delta \quad (43)$$

$$= \sqrt{e^{2\zeta(t^*)} - 1} \epsilon + \delta \quad (44)$$

Assuming that the norm of the score function $s_w(x, t)$ is bounded by a constant $\frac{1}{2} C_{s_w}$ and $\epsilon \sim \mathcal{N}(0, I)$, we have,

$$|\hat{x}_0 - x| \leq \left| \sqrt{2(e^{2\zeta(t^*)} \epsilon + \delta)} \right| + \zeta(t^*) C_{s_w} \quad (45)$$

Since $|\epsilon|^2 \sim \mathcal{X}^2(d)$, from the concerntartion inequality, we have

$$\Pr(|\epsilon|^2 \geq d + 2\sqrt{d\sigma} + 2\sigma) \leq e^{-\sigma} \quad (46)$$

Let $e^{-\sigma} = \varpi$, we get

$$\Pr\left(|\varpi|^2 \geq \sqrt{2d + 4\sqrt{d \log \frac{1}{\varpi}} + 4 \log \frac{1}{\varpi}}\right) \leq \varpi \quad (47)$$

Since $\hat{x}_0 - a$ occupies several dimensions within $\hat{x} - x$, their L1-norm should satisfy $|\hat{x}_0 - a| \leq |\hat{x}_0 - x|$. Therefore, combining Eq. 32 and Eq. 35, with the probability at least $1 - \varpi$, we have

$$D_{TV}(\rho_{\pi_o}(x), \rho_{\hat{\pi}_o}(x)) \leq L(|\delta| + \sqrt{e^{2\zeta(t^*)} - 1} C_{\varpi} + \zeta(t^*) C_{s_w}) + C \quad (48)$$

where the constant $C_{\varpi} = \sqrt{2d + 4\sqrt{d \log \frac{1}{\varpi}} + 4 \log \frac{1}{\varpi}}$.

C Proof for Theorem 3

Theorem 3. *For the purified demonstration distribution $\rho_{\hat{\pi}_o}(x)$ and clean demonstration distribution $\rho_{\pi_o}(x)$, we bound their policy value gap as follows,*

$$V_{\pi_o} - V_{\hat{\pi}_o} \leq \frac{R_{max}}{(1 - \gamma)^2} [L(|\delta| + \sqrt{e^{2\zeta(t^*)} - 1} C_{\varpi} + \zeta(t^*) C_{s_w}) + C], \quad (49)$$

where R_{max} denotes the upper bound of $r(x)$ for $\forall x$ and γ is the discounted rate.

Proof. According to Definition 2 in the paper, the policy value can be formulated as $V_\pi = \frac{1}{1-\gamma} \mathbb{E}_{(s,a) \sim \rho_\pi} [r(s,a)]$. Therefore, the policy gap between two policy π_o and $\hat{\pi}_o$ can be expressed as,

$$V_{\pi_o} - V_{\hat{\pi}_o} = \frac{1}{1-\gamma} \mathbb{E}_{(s,a) \sim \rho_{\pi_o}} [r(s,a)] - \frac{1}{1-\gamma} \mathbb{E}_{(s,a) \sim \rho_{\hat{\pi}_o}} [r(s,a)] \quad (50)$$

$$\leq \frac{1}{1-\gamma} \sum_{s,a \in \mathcal{S} \times \mathcal{A}} [(\rho_{\pi_o} - \rho_{\hat{\pi}_o}) r(s,a)] \quad (51)$$

$$\leq \frac{2R_{max}}{1-\gamma} D_{TV}(\rho_{\pi_o}, \rho_{\hat{\pi}_o}) \quad (52)$$

Combined with Theorem 2, we can bound $V_{\pi_o} - V_{\hat{\pi}_o}$ as follow,

$$V_{\pi_o} - V_{\hat{\pi}_o} \leq \frac{2R_{max}}{1-\gamma} \left[L(|\delta| + \sqrt{e^{2\zeta(t^*)} - 1} C_{\varpi} + \zeta(t^*) C_{s_w}) + C \right] \quad (53)$$

D Experimental Details

We will release the source code and all training data after the acceptance of this work.

D.1 Implementation Details of Diffusion Model

The architecture of diffusion model ϕ is five linear layers with a 0.2 dropout ratio, batch normalization, and ReLU nonlinear activation, and the size of the hidden dimension is 1024. We implement the above two algorithms based on this repo (<https://github.com/abarankab/DDPM>). The training epoch is set to be 10000 and the learning rate of ϕ is set to 1e-4. We set $T = 1000$ for all experiments and set the forward process variances to constants increasing linearly from $\beta_1 = 1e-4$ to $\beta_T = 0.02$.

D.2 Implementation Details of Imitation Learning

We use a deep neural network that has two 100×100 fully connected layers and uses Tanh as the activation layer to parameterize policy. To output continuous action, agent policy adopts a Gaussian strategy, hence the policy network outputs the mean and standard deviation of action. The continuous action is sampled from the normal distribution formulated with the action's mean and standard deviation. For online imitation learning methods, the discriminator and value function are using the same architecture as the policy network.

In offline imitation learning, the policy is trained with batch size 256, and the total epoch is set to be 1000. For online imitation learning, the learning rate of the discriminator D_ψ and the critic r_ψ is set to 3×10^{-4} . Five updates on the discriminator follow with one update on the policy network in one iteration. For the value function, the learning rate is set to 3×10^{-4} and three training updates are used in one iteration. We conduct the on-policy method TRPO [39] as RL step in online imitation learning, the learning rate is set to 3×10^{-4} with batch size 5000. The discount rate γ of the sampled trajectory is set to 0.995. The τ (GAE parameter) is set to 0.97.

D.2.1 Data Collection

We provide **five** imperfect demonstration datasets (from D1 to D5) to evaluate the performance of DP-IL on 4 MuJoCo tasks. After we train an optimal policy π_o by TRPO, we use **two** different kinds of ways to collect imperfect demonstration data in our experiments. The quality of imperfect demonstrations is provided in Table 6.

The **first** way to collect imperfect demonstrations is to add different Gaussian noise ξ to the action distribution a^* of π_o to form non-optimal policy π_n . The action of π_n is modeled as $a \sim \mathcal{N}(a^*, \xi^2)$ and we choose $\xi = [0.6, 0.4, 0.25]$ to generate imperfect demonstrations datasets **D1**, **D2** and **D3**. This imperfect demonstration collection way has been used in several works [12, 49].

The **second** way to collect imperfect demonstrations is to save checkpoints during the RL training of π_o . In our experiment, the RL training is conducted with 5M interactions with the environment. We save 2 checkpoints at 1.5M and 3M interactions to sample **D4** and **D5** datasets. This imperfect demonstration collection way has been investigated in [21, 38].

Table 6: The quality of demonstrations in 4 MuJoCo tasks, which is measured by the average cumulative reward of trajectories.

Task	\mathcal{S}	\mathcal{A}	D1	D2	D3	D4	D5
Ant	\mathbb{R}^{111}	\mathbb{R}^8	-73	227	3514	1570	2743
HalfCheetah	\mathbb{R}^{17}	\mathbb{R}^6	567	1090	1853	1491	2587
Walker2d	\mathbb{R}^{17}	\mathbb{R}^6	523	467	4362	1699	2717
Hopper	\mathbb{R}^{11}	\mathbb{R}^3	699	1037	3229	2153	3282

We sample 50 optimal demonstrations from ρ_{π_o} to train the diffusion model and 500 imperfect demonstrations from the imperfect demonstration dataset. For a fair comparison, all methods use both optimal and imperfect demonstrations to conduct imitation learning.

D.3 Compared Methods

We compare DP-IL with several *state-of-the-art* imitation learning with imperfect demonstration methods. Specifically, several offline imitation learning methods (*i.e.*, BCND [12] and DWBC [36]) and online imitation learning methods (*i.e.*, 2IWIL [38], IC-GAIL [38] and WGAIL [21]) are compared. We briefly review the details of methods compared against DP-IL in our experiments.

BCND [12] and DWBC [36] We follow the instructions to implement BCND since there is no official code available. Notice that for a fair comparison with other offline imitation learning methods, we do not use ensemble policies for BCND.

D-REX [37] We re-implement D-REX based on the official PyTorch code (<https://dsbrown1331.github.io/CoRL2019-DREX/>). In D-REX, the preference label of two trajectories is determined by the noise level of their corresponding demonstrators. Within imperfect demonstration datasets, we collect 5,000 random pairs of partial trajectories of length 50. We train the reward network using the Adam optimizer with a learning rate of 1e-4 and a batch size of 64 for 5000 iterations.

2IWIL and IC-GAIL [38] We re-implement 2IWIL/IC-GAIL based on the official implementation (<https://github.com/kristryer/Imitation-Learning-from-Imperfect-Demonstration>). In 2IWIL and IC-GAIL, a fraction of imperfect expert demonstrations are labeled with confidence (*i.e.*, $\mathcal{D}_l = \{(s_i, a_i), r_i\}_i^{n_l}$), while the remaining demonstrations are unlabeled (*i.e.*, $\mathcal{D}_u = \{(s_i, a_i)\}_i^{n_u}$). Since we have no access to the confidence score of the state-action pair in our setting, we use the normalized reward of the demonstrator as the confidence score for their related demonstrations. In the experiment, we choose 20% labeled demonstrations to train a semi-supervised classifier and then predict confidence for other 80% unlabeled demonstrations.

WGAIL [21] WGAIL is proposed to estimate confidence in GAIL framework without auxiliary information. The confidence $w(s, a)$ of each demonstration is calculated by $[(1/D_w^*(s, a) - 1)\pi_\theta(a|s)]^{\frac{1}{\beta+1}}$. The confidence estimation and GAIL training interact during the training. Followed with the official implementation (<https://github.com/yunke-wang/WGAIL>), β is set to be 1.